Experimental investigation of forces along anchors subjected to dynamic loading under tension and compression in field tests

Authors: Katharina M. Platzer 1, Corinna Wendeler 2, Rico Brändle 2, Martin Stolz 1

1. Bern University of Applied Sciences, Pestalozzistrasse 20, 3401 Burgdorf, Switzerland

   e-mail: katharina.schwarz-platzer@bfh.ch, martin.stolz@bfh.ch

2. Geobrugg AG, Aachstrasse 11, 8590 Romanshorn, Switzerland

   e-mail:corinna.wendeler@geobrugg.com, rico.braendle@geobrugg.com

Corresponding author: Katharina M. Platzer (e-mail: katharina.platzer@bfh.ch, tel: +41 344 264 145, fax: +41 344 264 43 08)

Abstract 200 words

Full-scale field tests of dynamic rockfall have been performed on a flexible SPIDER Avalanche System to study the dynamic force distribution along the foundations under dynamic loading. Therefore, an anchor to measure dynamic tensile forces and a pile to measure dynamic compressive forces were each equipped with strain gauges. Furthermore, a static pull loading test with load steps of one-minute duration was performed on the anchor to highlight the difference between dynamic and static loading. Effective kinetic energies applied on the net of the SPIDER Avalanche System range from 25 to 492 kJ with impact velocities between 17 and 25 m/s. The results show that the dynamic forces close to the pile- and anchor head are higher and that they are decreasing with increasing distance of pile and anchor. However, the dynamic tensile force distribution is non-linear over the length of the anchor, whereas the dynamic compressive force distribution is linear along the pile length. The comparison of static and dynamic tensile forces shows that dynamic tensile forces are depleted within a shorter distance of the anchor compared to the static tensile forces. Dynamic tensile forces present 25% less in value than the static tensile forces.

Keywords 4-6

Dynamic force, rockfall, field test, static pull loading test, kinetic energy, strain gauge

1. Introduction

Foundations are an essential part of protection structures as they transmit the occurring loads from the upper structure into the soil. Such structures are able to withstand static snow pressure as well as dynamic rockfall or debris flow impacts. In the last decades, a lot of effort has been invested to improve and strengthen the upper structure to stop rockfall successfully, achieving kinetic energies of 10’000 kJ for flexible rockfall protection structures and 500 kJ for flexible avalanche protection structures. Field measurements of rope forces due to rockfall impacts are used to dimension the foundations. However, the dimensioning of anchors and piles is calculated considering the forces to be only static. So far, no effort has been made to improve the dimensioning of the foundations due to dynamic impacts and to investigate a more appropriate load transfer concept. Even in the Guideline for European Technical Approval of Falling Rock Protection Kits, also known as ETAG 027 (EOTA 2013), which outlines the testing procedures for rockfall barrier systems, the foundation is excluded, since it is not considered part of the system. Therefore, a general lack of understanding regarding load transfer between foundations and soil, as well as system capacity, remains a fundamental obstacle for design. First aspects of a kind of safety concept on the anchor design are given in the ONR 24810 (ONR 2017), where the forces of the upslope anchors are summarized as a scalar. Hence, there is a need to quantify the different behaviour between static and dynamic load transfer along anchors and piles.

Anchors, typically frictional bolts, and flexible rope anchors are used as foundation part of a flexible avalanche prevention structure, made from high-tensile spiral rope nets (SPIDER® Avalanche, company Geobrugg AG). During winter, those prevention structures are subjected to static loads from the snow cover preventing the initiation of snow avalanches on steep slopes. Once snow cover has melted away, the flexible avalanche prevention structures are able to provide efficient protection against rockfall. A significant difference between a flexible SPIDER Avalanche System and a flexible rockfall barrier is the absence of braking elements. Due to the elasticity of the constructed net, the SPIDER Avalanche System can withstand highly dynamic rockfall events without damage. However, measurements of forces within these types of foundations during dynamic loading as well as the distribution into the soil are still missing. Although, there is an increasing amount of studies on energy-

absorbing rockbolts (Li et al. 2014; Kabwe and Wang 2015) which focus on dynamic solicitations, only few studies are reported on conventional frictional anchors. Many studies performed until now have been conducted in laboratory (Ansell 2005; Li 2012) or analysed with numerical methods (Mortazavi et al. 2013; Tong-bin Zhao et al. 2015; St.-Pierre et al. 2009; Ivandić 2003) as in situ experiments with dynamic loadings are cost expensive and present restrictions. Tests performed with Distributed Optical Sensing to measure static axial loading of a fully grouted rock bolt reveal that the measured axial strain along the rock bolt is exponential in form (Hyett 2013). Arndt (2014) and Turner (2009) performed vertical drop tests on various barrier fence systems, as well as post and post foundation direct impact tests, where the forces on the base of the posts were recorded. Ostermayer (1977) performed static pull out tests on anchors, which were instrumented with strain gauges and described the time dependent redistribution of friction forces along the anchor showing that forces change due to the rheological properties of soil. Shu (2005) performed field tests with different anchor types and found that the deformation of anchor heads under vertical tensile loading is non-linear. The authors state that the overall stability of a protection system is critically dependent on the performance of the anchors. Furthermore, it is pointed out that present knowledge of anchors is limited to pullout failure and empirical guidelines. Therefore, the study of in situ behaviour of frictional anchors under dynamic loading is necessary. With this knowledge, the elaboration of a new dimensioning concept, which considers the force distribution along anchors under dynamic loading in combination with a probabilistic model to reduce the anchor dimensions, as well as a safety design for dynamically loaded anchors, will lead to a more economical design of anchors. The objective of this research is to investigate the load distribution along the anchors of a flexible structure due to dynamic loading from rockfall in field tests. The study focuses on the fundamental issue related to the comparison of dynamic and static loading behaviour of the foundations, independently from the type of upper structure.

2. Experimental setup, instrumentation and analysis

The field tests were performed at the DTC Dynamic Test Centre AG in Vauffelin (Switzerland) following the Guideline for European Technical Approval of Falling Rock Protection Kits (ETAG027 2013). A flexible avalanche protection structure, the SPIDER Avalanche System, was set up. It has a modular design and consists of swivel posts, pressure plates, guy ropes, anchors and SPIDER spiral rope nets as the supporting flexible surface. Four posts were set up with a horizontal distance of 3.5 m between each of them. The posts are placed on pressure plates. The top of the posts are anchored via guy ropes downhill to ground anchors. The SPIDER spiral rope net is fixed on the top of the posts and anchored uphill to ground anchors. The overall height of the protection structure is 3.5 m. As the SPIDER Avalanche System is initially designed to prevent the initiation of an avalanche, it is not equipped with dissipating devices. An overview of the flexible avalanche prevention structure and its foundations is given in Figure 1.

Figure 1 Schematic side view of a SPIDER Avalanche System. The arrows mark the directions of loading along the instrumented pile (compression) and anchor (tension). a) shows the front view of the experiment.

Due to the structural behaviour of the SPIDER avalanche system, a dynamic impact into the net invokes compressive forces along the swivel posts and the pressure piles underneath and tensile forces along the guy ropes and its anchors underneath.

The pressure pile and anchor of the impact zone of the SPIDER Avalanche System were built as micro piles. They consist of a hollow round steel bar with a ribbed steel tube, which is grouted over its whole length. Therefore, it guarantees a mechanical interlocking with the surrounding soil. In its hollow area of 26 mm diameter, a thin steel bar was implemented. On the thin steel bar four strain gauges were glued and protected with a special kit. The outer diameter of the round steel bar is 52 mm and after grouting the diameter of the cased micro pile was d = 100 mm. The cross-section of the micro piles is shown in Figure 2. Note that only under one of the posts of the impact zone of the SPIDER Avalanche System the foundation was performed as pile. This pile was set to get measurements of dynamic compressive forces. The other posts have ground plates to distribute the forces into the soil.

Concerning the pressure pile, the effective cross-sectional area consists of the area of the steel rod and the area of the circumfluent grout (A_c = 7854 mm^2). For the anchor instead, which is loaded under tension, only the steel parts were considered and not the area of grout. Therefore, the cross-sectional area consists of the circular cross-sectional area of the steel bolt A_t and the small steel profile with the rectangular area A_s of 1274 mm^2, where the strain gauges are glued on. The modulus of elasticity for steel is given as E_s = 210 000 N/mm^2 and for the injection grout is E_c = 37 000 N/mm^2. The granularity of the injection grout is given as 0-0.5 mm. To calculate the forces from the strain gauges measurements, the cross section of grout area A_c is calculated as

$$A_c = r^2\pi - \left(A_t + A_s\right)$$

where r is the radius of the anchor's and pile's cross section.

With the relation of moduli of elasticity between steel and grout of $n = E_s/E_c$ and

$$f = \left(\frac{A_c}{n} + A_t + A_s\right) * E_s * 10^{-3}$$

we calculate the tensile or compressive force F [kN]

$$F = f * \varepsilon * 10^{-6}$$

where ε is the recorded elongation of the strain gauge.

One of the posts of the impact zone of the SPIDER Avalanche System was equipped with a strain gauge full bridge, located ca. 60 cm above the ground. The post was built as a swivel support and placed on the squared ground plate with a side length of 250 mm. In order to record the dynamic behaviour of forces under compression, in the elongation of the post a pressure pile with 75° of inclination and a length of 5.215 m was set into the soil (see Figure 1). The pile was dimensioned after the technical guideline of avalanche supporting structures in the starting zone due to static snow loads (Margreth

2007). The pile was equipped with four strain gauges along its length. The positions of strain gauges (DMS 1 to DMS 4) are seen in Figure 2. The instrument cables of the strain gauges were led through the centre of the pressure pile into the anchor head and then out of the ground plate laterally.

Additionally, the forces in the downhill rope, which anchors the SPIDER Avalanche System from the top of the swivel support to the ground, was recorded with a force cell. The force cell is placed between the end of the rope and the head of the anchor. In elongation of the rope, an anchor with 45° of inclination to the horizontal and a length of 5.105 m was set and equipped with four strain gauges (positions see Figure 2).

All dynamic load experiments were recorded with a high-speed camera, taking 500 frames per second. Normed EOTA (European Organization for Technical Assessment) blocks with a mass from 335 kg to 3238 kg were accelerated with a modern sledge installation and then thrown into the net. Through retarding the sledge with a bending iron brake, the block falls off its mounting and topples in a free fall over a distance of about six meters into the centre of the net. By analysing the high-speed movies, the impact height and impact speed were established. To determine the trajectory, the forces and the energy absorption, the accelerations of the EOTA-block in its centre of gravity were measured, using two three-axis accelerometers (2000 g) and an angular velocity sensor (9000 °/s). The measurement frequency was performed with 20 kHz.

Figure 2 Left: Schematic picture of the pressure pile with specification of the positions of the strain gauges. The total length of the pile is 5215 mm. Upper Right: schematic cross-section of pressure pile and anchor. The steel rod with the strain gauges glued on it, is placed in the centre. Lower Right: Photo of grouted anchor with the measurement cables coming out at the anchor head.

The sampling rate of the force measurements was recorded with 4.8 kHz using a special software and a measurement amplifier (HBM Spider 8).

Furthermore, a static pull loading test was performed on the same instrumented anchor of the SPIDER Avalanche System, which was monitored during the dynamic tests. Seven force loading steps ranging between 50 kN and 250 kN were applied to the anchor head with a hydraulic pull load press for a duration of one minute each. Along the anchor, the applied static forces were recorded with the same setup of instrumentation and positions of strain gauges as for the dynamic tests. The results of static loading are compared with the dynamic forces in section 3 “Results and Discussion”.

Soil properties were determined in the laboratory with probes taken from the field. A grain size distribution analysis after USCS classification was performed to get the characteristic soil properties. The soil material is characterized as fine to coarse gravel, silty sandy with an internal angle of friction of 42°, cohesionless. The soil density was investigated with two Standard Penetration Tests (SPT, 63kg hammer weight and 75 cm falling height of the weight). The SPT values are shown in the appendix (Figure A1). The soil was homogenous within depths from 1 to 6 meters with a number of 5 hits per 10 cm penetration depth. Over the whole depth no groundwater was apparent.

Note that within the full-scale field tests the focus was put on the dynamic load transfer per se along the anchor and pressure pile and not on the symmetry of load transfer based on the impact zone of the SPIDER avalanche net nor on the load transfer behaviour of the SPIDER Avalanche System.

The mean force F_{mean} acting on the net was determined from the effective kinetic energy absorbed of the net and the maximum deflection of the net due to the impact of the block where $F_{mean} = E/s$. F_{mean} is used to compare the overall impact energy of each experiment to the forces measured in the anchor and pile. E is the kinetic energy [kJ] and s is the maximum deflection of the net in [m]. The effective absorbed kinetic energy of the net [kJ] is calculated from the product of the dynamic force F_a in x-direction and the dynamic deformation s in x-direction. Thereby the dynamic force F_a is calculated by the product of the acceleration a of the block in x-direction times the mass m of the block. The dynamic deformation s is calculated from the integral over the acceleration a_x. In case the net broke (experiments 3, 4 and 7), the maximum dynamic deformation is taken at the position of the maximum acceleration of the block.

3. Results and Discussion

3.1. General overview of the experiments

In total seven experiments have been performed in the field, wherein the applied kinetic energies of the block on the SPIDER Avalanche System ranged from 56 kJ to 518 kJ (Murri and Uhr 2011a; Murri and Haldimann 2011b; Murri and Uhr 2011c; Murri and Uhr 2012). As the SPIDER Avalanche System did not always withstand the kinetic impacts of the block, the effective kinetic energies absorbed of the net ranged between 25 kJ and 492 kJ (see Table 1 and Table 2). Impact velocities of the EOTA block ranged between 17 and 25 m/s.

Experiment 1, 2 and 3 were performed during the same day in May 2011. Experiment 1 was charged with 56 kJ and experiment 2 with a kinetic energy of 108 kJ. During both experiments the Avalanche System could hold back the block without being destroyed. Within the third experiment the SPIDER Avalanche System was charged with an applied kinetic energy of 165 kJ, which resulted in an effective kinetic energy of only 25 kJ to the System as the net broke. For experiment 4, a new SPIDER Avalanche System was set up with a modified net and tested in September 2011 with an applied kinetic energy of 203 kJ. There, the net broke but could hold an effective kinetic energy of 141 kJ. Again, a new System with a modified net was set up in November 2011, which held the block of experiment 5 with an effective kinetic energy of 202 kJ. Within the second impact of experiment 6 the effective kinetic energy was 298 kJ and the flexible net held the block. In April 2012 a SPIDER Avalanche System was set up for experiment 7 and was charged with an applied kinetic energy of 518 kJ, which resulted in an effective kinetic energy of 492 kJ on the System as the net broke. Note that the SPIDER Avalanche System was subjected to multiple impacts in the experiments Nr. 2, 3 and 6, which means that the net has already been deflected before. In order to be able to compare the deflections of the net from all experiments, the deflections are analysed from theoretical first contact with the uninfluenced net.

All four strain gauge measurements (DMS) along the pile worked well for the first three experiments.

From experiment 4 on, strain gauge number 3 stopped working and from experiment 5 on, strain gauge number 2 ceased. The cables of strain gauges 2 and 3 were cut by the ground plate of the post during demounting and remounting of the SPIDER Avalanche System, explaining the loss of signal of these two strain gauges. In the case of the strain gauge measurement along the anchor, strain gauge number 2 did not work during any experiments. We attribute this loss of signal to the fact that during the installation of the steel bar into the micro pile or during grouting the strain gauge must have been damaged. From experiment 7 on, strain gauge 1 stopped working. Note that all strain gauges in the anchor and pressure pile remained outside for one year and were subjected to harsh weather conditions. Due to the dynamic impact of the block into the SPIDER Avalanche System the strains in the downhill rope, in the pile and along the anchor as well as the pile were recorded over time and then converted into forces. Table 1 gives an overview of the measured impact energies and maximum dynamic forces for the post and the pile**.** The negative values represent compressive forces. Table 2 gives an overview of the measured impact energies and maximum dynamic forces for the rope and the anchor.

Figure 3 Time history of the measured dynamic compressive force distribution for the post and along the pile for experiment 2 with an effective absorbed kinetic energy of 108 kJ.

Figure 3 shows the force distribution over time for Experiment 2 with a kinetic impact energy of 108 kJ on the net. The force in the post is depicted over time and underneath the strain gauges DMS 1 to DMS 4 along the pile. The decrease of force with increasing depth along the pile can clearly be seen. The impact of the block to the net lasts about 0.3 ms, then the block gets thrown back from the elastic net. The second peak, which lasts about 0.6 ms is due to the elastic reaction of the SPIDER Avalanche System. The same behaviour is visible in case of the tensile forces in the downhill rope and along the anchor (see Figure A3 in the appendix) and is consistent for all measurements.

3.2. Force distribution along the pile under compression

The distribution of dynamic forces is investigated as compression loading along the pile. Figure 4 shows the measured dynamic forces under compression for the post, as well as along the length of the pile, for the seven experiments (56 kJ to 492 kJ). The distribution of axial dynamic forces along the pile shows a linear decrease of forces with increasing distance along the pile. Close to the pile head the dynamic compressive forces are highest and they are decreasing gradually with increasing distance along the pile. By increasing the kinetic energy, the increase of forces close to the pile head is much bigger compared to the increase of forces towards the end of the pile. With the increase of kinetic energy, the slope line of the linear regression becomes steeper. The ground plate, which is situated under the post, depletes around 50% of compressive force (for impact energies between 56 and 200 kJ) and around 35 % of compressive force for the experiments with kinetic energies between 300 and 490 kJ. Those measurements (see Table 1, Figure 4 and Figure 6) reveal that the ground plate, which is situated at the lower end of the post, namely at the soil surface, transfers a certain amount of applied forces from the post via its contact area into the soil. Therefore, the values of dynamic compressive forces are disproportionally smaller in the pile head compared to the values in the post. With impact energies up to 492 kJ the dynamic compressive forces are already depleted at two third of the pile

length.

Figure 4 Measured maximum dynamic compressive forces on the foot of the post and along the pile for seven experiments with effective absorbed kinetic energies of the net. m' and m'' indicate that those experiments are multiple impacts of the setup of experiment m. n' indicates that the experiment is a multiple impact of the setup of experiment n.

In Figure 5 the percentagewise load distribution for compressive loads is depicted versus the distance along the pile. The measured forces on the post correspond to 100% each and the forces along the pile are set in relation to the measured force in the post. On the position of DMS 4 the dynamic compressive forces of all experiments are less than 3% of the maximum force measured in the post.

The percentagewise load transfer from the pile to the soil is, for all experiments, consistent due to the difference of the E moduli of the pile and the soil and due to the bonded friction of the injection grout with the soil. Therefore, the major part of forces is getting depleted close to the pile head and the activated friction between pile and soil along the whole length of the pile is proportional to the applied load. This shows that a length of effective anchorage is evident.

Figure 5 Percentage of the maximum compressive force along the length of the pile for effective absorbed kinetic energies of the net. The reference value, where the 100 percent are attributed to, is the force measured in the post. m' and m'' indicate that those experiments are multiple impacts of the setup of experiment m. n' indicates that the experiment is a multiple impact of the setup of experiment n. A linear regression is calculated for the measurements with minimum three points and the multiple R squared values are shown in the legend.

Figure 6 Maximum dynamic compressive forces of the post and the pile over the kinetic impact energy. A linear regression is calculated for the measurements with minimum three points and the multiple R squared values are shown in the legend.

For the dimensioning of piles, it is important to know how much force is transferred from the net into the foundations during an impact. Figure 6 shows the change of the maximum dynamic compressive forces under different input kinetic energies. With increasing kinetic energy, the dynamic forces in the post as well as in the pile increase linearly. Within the same kinetic energy, the forces at the end of the pile are lowest and they are increasing towards the pile head. As shown above, the forces measured on the post are higher than along the pile. Although the measurements in the post are close together for experiment 4 with a kinetic energy E_{kin} of 141 kJ and experiment 5 with E_{kin} of 200 kJ respectively, the force on DMS 1 is much smaller for the higher input kinetic energy of experiment 5 than of experiment 4. We attribute this fact to the setup of the SPIDER Avalanche System, which provides slightly different boundary conditions after each new setup. As only one of the impact zone posts is equipped with measurement devices we cannot guarantee a symmetric loading of both impact zone posts. In experiment 4 the equipped post was obviously loaded with comparatively higher forces than during the other experiments. This fact can also be confirmed by the video analysis, where the more tensioned

downhill rope on the side of the equipped swivel post in comparison to the other side of the unequipped post is visible.

The force F_{mean} acting on the net was determined from the effective energy absorbed from the net and the maximum deflection of the net due to the impact of the block with $F_{mean} = E/s$, where E means the kinetic energy [kJ] and s the maximum deflection of the net in [m].

3.3. Force distribution along the anchor under tension

In this section we analyse the distribution of dynamic tensile forces along the anchor. Figure 7 shows the measured dynamic tensile forces along the distance of the anchor. The dynamic tensile force distribution shows a non-linear behaviour. Whereas close to the anchor head the forces are highest, they are decreasing non-linearly over the distance of the anchor. Towards the anchor head, the increase of forces due to an increase in impact energy is more pronounced than towards the end of the anchor. The dynamic forces of an impact less than 56 kJ are depleted completely within the first 3.5 m of the anchor. With a kinetic impact of 492 kJ at the end of the anchor a dynamic tensile force of 10 kN is still present. Expressed in percentage, about 20% of the forces remain at the end of the anchor for a kinetic energy of 492 kJ. Zhao 2015 has measured a similar behaviour of the distribution of the dynamic tensile forces along an anchor.

Figure 7 Measured maximum dynamic tensile forces on the rope and along the anchor for seven experiments with effective absorbed kinetic energies of the net. m' and m'' indicate that those experiments are multiple impacts of the setup of experiment m. n' indicates that the experiment is a multiple impact of the setup of experiment n.

In Figure 8 the percentagewise load distribution for tensile loads is depicted versus the distance of the anchor. The measured forces in the downhill rope correspond to 100% each and the forces along the anchor are set in relation to the measured force in the downhill rope. On the position of DMS 4 the dynamic tensile forces of all experiments range between 1-20% of the maximum force measured in the downhill rope. Although data from the strain gauge DMS 2 are missing, we see a non- linearly decreasing force distribution over the length of the anchor. The comparison of force percentages between different experiments highlights, that with the smallest kinetic energy of 56 kJ, the forces are already depleted at 3.25 m depth of the anchor. For higher kinetic energies the forces reach already the end of the anchor in around 5 m depth in the range of 4 to 18% percent, depending on the amount of dynamic loading.

Figure 8 Percentage of the maximum tensile force along the length of the anchor for experiments with effective absorbed kinetic energies of the net. The reference value, where the 100 percent are attributed to, is the force measured in the downhill rope. m' and m'' indicate that those experiments are multiple impacts of the setup of experiment m. n' indicates that the experiment is a multiple impact of the setup of experiment n.

The change of maximum dynamic tensile forces under different input kinetic energies from 25 kJ to 492 kJ is shown in Figure 9. With increasing kinetic energy, the forces in the downhill rope, as well as in

the anchor, increase linearly. Within the same kinetic energy, the forces at the end of the anchor are lowest and they are increasing towards the anchor head. The tensile forces measured in the downhill rope are higher than the tensile forces along the anchor. The dynamic forces of DMS 1 and of the downhill rope F_{rope} are smaller for a kinetic energy of 56 kJ than for the lower effective kinetic energy of 25 kJ. This fact is due to the multiple impact on the same SPIDER Avalanche System as the first experiment was conducted with a kinetic energy of 56 kJ. Due to the first impact of the block the upper construction of the flexible Avalanche System got influenced and the initial elasticity of the net got reduced due to plastic deformations from the first impact. Therefore, the flexible Avalanche System and the ropes have implemented a deformation due to the impact and are not tensioned anymore compared to the initial situation. The load distribution along the anchor seems to behave differently from experiment 3, as we do not observe a pronounced decrease in forces from DMS 3 to DMS4.

Figure 9 Maximum dynamic tensile forces in the downhill rope and the anchor over the kinetic impact energy. A linear regression is calculated for the measurements with minimum three points and the multiple R squared values are shown in the legend.

3.4. Comparison between tensile and compressive loading

The comparison of dynamic force distribution for tensile and compressive loading along the anchor and pile does not show the same tendency. We attribute the linear distribution of compressive forces along the pile to the stiffness of the pile. A schematic overview of this behaviour is shown in the appendix (Figure A2). The whole cross-sectional area of the grouting material is loaded. The stiffness of the grouted pile is some order of magnitudes higher than the stiffness of the soil. In the case of dynamic tensile force distribution along the anchor, the cross-sectional area of the grouting material is not considered, as the tensile stiffness of grout is already exceeded within the smallest kinetic impact energy. Therefore, only the very small cross-sectional area of steel is considered and leads to a non-linear decrease of tensile forces along the length of the anchor. A schematic overview of this behaviour is shown in the appendix (Figure A2).

Due to the effective area of the ground plate, a part of dynamic forces is depleted through its effective area, which results in a lower dynamic compressive force value compared to the dynamic tensile force. Furthermore, as the effective area of the pile is larger (due to the grout area) than in the case of the anchor, the compressive forces are depleted within a smaller distance. In case of tensile loading, the dynamic forces diminish from anchor head to the anchor end in a non-linear way. There, only the effective area of steel is considered and leads to a non-linear decrease of tensile forces along the length of the anchor.

The maximum forces measured in the anchor and in the pile are proportionally smaller than the maximum forces in the downhill rope and post situated above. In all seven experiments the downhill rope was exposed to the smaller amount of forces than the swivel post and therefore the absolute force values are smaller along the anchor than in the pile. This fact is due to the setup of the whole avalanche structure.

Due to the structural behaviour of the SPIDER Avalanche System the post and pile were subjected to

higher forces, which are around 60% higher than the forces in the downhill rope and the anchor. However, the compressive forces, which have higher absolute values than the tensile forces in the anchor, are depleted within a shorter distance along the pile. By introducing F_{mean}, which is acting on the SPIDER Avalanche System, this mean force brings the dynamic forces along the post and the downhill rope in relation to the whole system. Whereas F_{mean} is higher compared to the dynamic forces in the downhill rope and the anchor (see Figure 6), it is within the same range of dynamic forces in the post and the head of the pile (Figure 9).

3.5. Comparison between static and dynamic loading

A static pull loading test was performed on the anchor. Each force loading step imposed on the head of the anchor was kept constant for one minute. The recorded static force values along the anchor were taken at the end of each loading step and compared with the forces due to dynamic impact from the rockfall. Therefore, the measured dynamic force in the downhill rope was defined as reference value and compared to the similar static loading value from the pull loading test (the absolute force values of the static pull loading test as well as the normalised force values of static pull loading are shown in the appendix, Figure A4 and Figure A5). Figure 10 shows the normalised tensile forces of dynamic and static measurement over the distance along the anchor. The normalised tensile force is calculated as quotient in percent between the measured force along the anchor and the measured force in the rope. The decrease of forces is supposed to be non-linear in the static case as well as in the dynamic case. However, due to the dynamic impact, the tensile forces are smaller than the static tensile forces, compared at the same position on the anchor. For a dynamic impact of 300 kJ onto the net, which corresponds to a dynamic force of 32 kN in the downhill rope, only 17% of the dynamic force are recorded in the lowest part of the anchor at 5 m depth. However, during the static pull loading test 26 % of the static forces are recorded at the same depth. A similar behaviour between dynamic and static forces is observed in the case where the anchor is tensioned with 64 kN by static loading, which corresponds to 60 kN dynamic loading (492 kJ). This result has a fundamental implication for the future design of foundations for rockfall and avalanche barriers, depending on the type of loading. Although it is not the objective of this paper to define a new design criteria, it is worth to mention that based on our results there is a linear relationship between the kinetic energy and the maximum dynamic tensile and compressive forces that could be used to design foundations. Obviously, specific tests for different combinations of factors (soiltype, foundation type, upper structure,...) are needed to define the design criteria.

In the dynamic case, the anchor behaves elastoplastically and the forces along the anchor are dissipated over a shorter length. In the static loading case, the anchor behaviour is more plastic, depending on the relaxation time of the soil-anchor frictional forces. This behaviour is described in the study of Ostermayer (1977), who measured the time dependent variation of frictional forces along an anchor during 300 minutes.

Figure 10 Experiment with 298 kJ: comparison of the static forces from the pull loading test with the dynamic forces from experiment 6 acting along the anchor

4. Conclusion

Full-scale field tests have successfully been performed under tension as well as under compression and the consequences of dynamic impacts on an anchor and a pile of a SPIDER Avalanche System were investigated for kinetic energies up to 492 kJ.

Based on the experiments we can conclude that:

- Dynamic compressive force distribution along a pile decreases linearly with increasing pile length.

- Dynamic tensile force distribution along an anchor decreases non-linearly with increasing anchor length.

- Dynamic tensile forces are depleted within a shorter distance of the anchor compared to the static tensile forces.

The axial force distribution along anchor and pile clearly differs between static and dynamic loading within a range of 25% for the investigated applied kinetic energies. The ground plate under the post depletes 35 to 50% of forces in the case of compressive loading. The results of this study show that for the optimization of foundation design in the case of flexible systems the type of loading should be considered. Specifically, for the dynamic loading shorter anchor lengths are needed compared to static loaded ones.

The experiments verified that all load carrying components of the SPIDER Avalanche System are reliable when dynamically loaded. Further performed experiments reveal that the SPIDER Avalanche System is able, with a modified net, to take up around 500 kJ of rockfall energy compared to traditional steel frame constructions, which can only absorb up to maximum 50 kJ. The presented data are the first results for such flexible systems and they highlight the need to make further investigations in order to develop a new dimensioning concept for foundations under dynamic loading.

Acknowledgements

The tests were performed at the Dynamic Test Center AG in Vauffelin, Switzerland, guided by Raphael Murri. The authors are grateful to the whole team around Mr. Murri and to Hans-Peter von Allmen and Ruedi Rüegsegger who helped installing the SPIDER Avalanche System.

References

Ansell, A. 2005. Laboratory testing of a new type of energy absorbing rock bolt. Tunneling and Underground Space Technology 20:291-300. doi: 10.106/j.tust.2004.12.001.

Arndt, B., Ortiz, T., and Group, B. 2014. Full Scale Testing of Rockfall Barrier and Post Foundation Systems. Rocky Mountain Geo-Conference.

EOTA 2013. ETAG 027 Guideline for European Technical Approval of Falling Rock Protection Kits. European

Organization for Technical Approvals (EOTA), Brussels, Belgium.

Hyett, A., Forbes, B., and Spearing, S. 2013. Enlightening Bolts: Using Distributed Optical Sensing to Measure the Strain Profile along Fully Grouted Rock Bolts. 32nd International Conference on Ground Control in Mining.

Ivandić, K., and Verić, F. 2003. Analysis of the geotechnical anchor load transfer mechanism. International 13th Conference on Soil Mechanics and Geotechnical Engineering, Praque, The Czech Republic.

Kabwe, E., and Wang, Y. 2015. Review on Rockburst Theory and Types of Rock Support in Rockburst Prone Mines. Open Journal of Safety and Technology, **5**: 104-121. doi: 10.4236/ojsst.2015.54013.

Li, C.C., and Doucet, C. 2012. Performance of D-bolts under dynamic loading conditions. Rock Mechanics Rock Engineering, **45(2)**: 193-204. doi: 10.1007/s00603-011-0202-1.

Li, C.C., Stjern, G., and Myrvang, A. 2014. A review on the performance of conventional and energy-absorbing rockbolts. Journal of Rock Mechanics and Geotechnical Engineering, 6: 315-327. doi:10.1016/j.jrmge.2013.12.008.

Margreth, S. 2007. Lawinenverbau im Anbruchgebiet. Technische Richtlinie als Vollzugshilfe. Umwelt-Vollzug Nr. 0704. Bundesamt für Umwelt, Bern, WSL Eidgenössisches Institut für Schnee- und Lawinenforschung SLF, Davos.

Mortazavi, A., and Alavi, F.T. 2013. A numerical study of the behavior of fully grouted rockbolts under dynamic loading. Soil Dynamics and Earthquake Engineering, **54**: 66-72. doi: 10.1016/j.soildyn.2013.08.003.

Murri, R., and Uhr, M. 2011a. Dynamische Prüfungen am Geobrugg Schutzzaunsystem SPIDER Avalanche mit einem 335 kg EOTA-Stein und einer 750 kg FIA-Kugel vom 31. Mai 2011. Bericht. Dynamic Test Center DTC, Vauffelin, Schweiz.

Murri, R., and Haldimann, M. 2011b. Dynamische Prüfungen am Geobrugg Schutzzaunsystem SPIDER Avalanche mit einem 1000 kg EOTA Stein vom 07. September 2011. Bericht. Dynamic Test Center DTC, Vauffelin, Schweiz.

Murri, R., and Uhr, M. 2011c. Dynamische Prüfungen am Geobrugg Schutzzaunsystem SPIDER Avalanche mit einem 1000 kg EOTA Stein vom 29. November 2011. Bericht. Dynamic Test Center DTC, Vauffelin, Schweiz.

Murri, R., and Uhr, M. 2012. Dynamische Prüfung am Geobrugg Schutzzaunsystem SPIDER Avalanche mit einem 3200 kg EOTA-Stein mit 500 kJ vom 18. April 2012. Bericht. Dynamic Test Center DTC, Vauffelin, Schweiz.

ONR 2017. ONR 24810 Technical protection against rockfall — Terms and definitions, effects of actions, design, monitoring and maintenance. Austrian Standards.

Ostermayer, H., and Scheele, F. 1977. Research on ground anchors in non-cohesive soils. *In* Proceedings of the 9th International Conference on Soil Mechanics and Foundation Engineering, Tokyo, Japan. Volume 97: pp.92-97.

Shu, S., Muhunthan, B., Badger, T.C., and Grandorff, R. 2005. Load testing of anchors for wire mesh and cable net rockfall slope protection systems. Engineering Geology **79**: 162-176. doi: 10.106/j.enggeo.2005.01.008.

St.-Pierre, L., Hassani, F.P., Radziszewski, P.H., and Ouellet, J. 2009. Development of a dynamic model for a cone bolt. International Journal of Rock Mechanics and Mining Sciences **46**(1): 107-144. doi: 10.1016/j.ijrmms.2008.05.005.

Turner, R., Duffy, J.D., and Turner, J.P. 2009. Post Foundations for Flexible Rockfall Fences. 60th Highway Geology Symposium, Buffalo, New York.

Zhao, T., Guo, W., Yin, Y., and Tan, Y. 2015. Bolt Pull-Out Tests of Anchorage Body under Different Loading Rates. Shock and Vibration, Hindawi Publishing Corporation. doi: 10.1155/2015/121673.

Appendix

In Figure A1 the result of a Standard Penetration Test (SPT) over a depth of 6 meters is presented. The amount of hits for 10 cm vertical displacement is depicted over the depth in m. The skin friction value of the tube is depicted with the dashed-dotted line.

Figure A1 Data obtained from the SPT test: The amount of hits for 10 cm vertical displacement is depicted over the depth in m. The skin friction value of the tube is depicted with the dashed-dotted line.

Figure A2 sows a schematic sketch of the stress distribution along the length of an anchor/pile during dynamic loading. With increasing distance along the pile the axial stress decreases linearly and the shear stress remains constant. With increasing distance along the anchor the axial stress and shear stress decrease non-linearly.

Figure A2 Schematic sketch of the stress distribution along the length of an anchor/pile during dynamic loading.

Figure A3 shows the force distribution over time for Experiment 2 in the downhill rope and along the anchor with strain gauges DMS 1 to DMS 4 with a kinetic impact energy of 108 kJ on the net. The decrease of force with increasing depth along the anchor can be seen clearly.

Figure A3 Time history of the measured dynamic tensile force distribution for the downhill rope and along the anchor for Experiment 2 with an effective absorbed kinetic energy of 108 kJ.

Figure A4 shows the measured maximum static tensile forces on the rope and along the anchor for each

loading step of the static pull loading test.

Figure A4 Measured maximum static tensile forces on the rope and along the anchor for each load step of the static pull loading test.

Figure A5 shows the percentage of the maximum static tensile forces on the rope and along the anchor for each load step of the static pull loading test.

Figure A5 Percentage of the maximum static tensile forces on the rope and along the anchor for each load step of the static pull loading test.

Table 1 Overview of all dynamic rockfall experiments performed with results of effective absorbed kinetic energy of the net, maximum deflection s of the net, acting force F_{mean} on the net and recorded maximum dynamic compressive forces in the post and along pressure pile (DMS 1 to DMS4). The negative values represent compressive forces.

Experiment Nr	1	2	3	4	5	6	7
Date	31.05.11	31.05.11	31.05.11	07.09.11	29.11.11	29.11.11	18.04.12
applied kinetic energy on the net [kJ]	56	108	165	203	202	298	518
Effective absorbed kin. energy of the net [kJ]	56	108	25	141	202	298	492
maximum deflection of the net s [m]	2.49	2.81	2.74	2.76	2.95	3.66	2.76
F_{mean} on net [kN]	22.5	38.4	9.4	51.1	68.5	81.4	148.5
Post max Force [kN]	-40	-54	-20	-125	-120	-140	-200
DMS 1 max Force [kN]	-19	-26	-10	-103	-63.4	-95.9	-125
DMS 2 max Force [kN]	-12	-16	-7	-80	no signal	no signal	no signal
DMS 3 max Force [kN]	-4	-5	-2	no signal	no signal	no signal	no signal
DMS 4 max Force [kN]	0	-1	-0.4	-2	-4.8	-5	noise

Table 2 Overview of all dynamic rockfall experiments performed with results of effective absorbed kinetic energy of the net, maximum deflection s of the net, acting force F_{mean} on the net and recorded maximum dynamic tensile forces in the downhill rope and along the anchor (DMS 1 to DMS4).

Experiment Nr	1	2	3	4	5	6	7
Date	31.05.11	31.05.11	31.05.11	07.09.11	29.11.11	29.11.11	18.04.12
applied kinetic energy on the net [kJ]	56	108	165	203	202	298	518
Effective absorbed kin. energy of the net [kJ]	56	108	25	141	202	298	492
maximum deflection of the net s [m]	2.49	2.81	2.74	2.76	2.95	3.66	2.76
F_{mean} on net [kN]	22.5	38.4	9.4	51.1	68.5	81.4	148.5
Rope max Force [kN]	3.6	19	10.3	12.3	17.5	32	60
DMS 1 max Force [kN]	noise	11	7.5	16.3	17.4	29.6	no signal
DMS 2 max Force [kN]	no signal	no signal	no signal	no signal	no signal	no signal	no signal
DMS 3 max Force [kN]	noise	~2.5	noise ~1	2.5	2.7	6.4	14.6
DMS 4 max Force [kN]	noise	~0.7	noise ~0.9	1.9	2.5	4.6	10

Figure Captions

Figure 1 Schematic side view of a SPIDER Avalanche System. The arrows mark the directions of loading along the instrumented pile (compression) and anchor (tension). a) shows the front view of the experiment.

Figure 2 Left: Schematic picture of the pressure pile with specification of the positions of the strain gauges. The total length of the pile is 5215 mm. Upper Right: schematic cross-section of pressure pile and anchor. The steel rod with the strain gauges glued on it, is placed in the centre. Lower Right: Photo of grouted anchor with the measurement cables coming out at the anchor head.

Figure 3 Time history of the measured dynamic compressive force distribution for the post and along the pile for Experiment 2 with an effective absorbed kinetic energy of 108 kJ.

Figure 4 Measured maximum dynamic compressive forces on the foot of the post and along the pile for seven experiments with effective absorbed kinetic energies of the net. m' and m'' indicate that those experiments are multiple impacts of the setup of experiment m. n' indicates that the experiment is a multiple impact of the setup of experiment n.

Figure 5 Percentage of the maximum compressive force along the length of the pile for effective absorbed kinetic energies of the net. The reference value, where the 100 percent are attributed to, is the force measured in the post. m' and m'' indicate that those experiments are multiple impacts of the setup of experiment m. n' indicates that the experiment is a multiple impact of the setup of experiment n. A linear regression is calculated for the measurements with minimum three points and the multiple R squared values are shown in the legend.

Figure 6 Maximum dynamic compressive forces of the post and the pile over the kinetic impact energy. A linear regression is calculated for the measurements with minimum three points and the multiple R squared values are shown in the legend.

Figure 7 Measured maximum dynamic tensile forces on the rope and along the anchor for seven experiments with effective absorbed kinetic energies of the net. m' and m'' indicate that those experiments are multiple impacts of the setup of experiment m. n' indicates that the experiment is a multiple impact of the setup of experiment n.

Figure 8 Percentage of the maximum tensile force along the length of the anchor for experiments with effective absorbed kinetic energies of the net. The reference value, where the 100 percent are attributed to, is the force measured in the downhill rope. m' and m'' indicate that those experiments are multiple impacts of the setup of experiment m. n' indicates that the experiment is a multiple impact of the setup of experiment n.

Figure 9 Maximum dynamic tensile forces in the downhill rope and the anchor over the kinetic impact energy. A linear regression is calculated for the measurements with minimum three points and the multiple R squared values are shown in the legend.

Figure 10 Comparison of the static forces from the pull loading test with the dynamic forces from experiment 6 and 7 acting along the anchor.

Figure A1 Data obtained from the SPT test: The amount of hits for 10 cm vertical displacement is depicted over the depth in m. The skin friction value of the tube is depicted with the dashed-dotted line.

Figure A2 Schematic sketch of the stress distribution along the length of an anchor/pile during dynamic loading.

Figure A3 Time history of the measured dynamic tensile force distribution for the downhill rope and along the anchor for Experiment 2 with an effective absorbed kinetic energy of 108 kJ.

Figure A4 Measured maximum static tensile forces on the rope and along the anchor for each load step of the static pull loading test.

Figure A5 Percentage of the maximum static tensile forces on the rope and along the anchor for each load step of the static pull loading test.

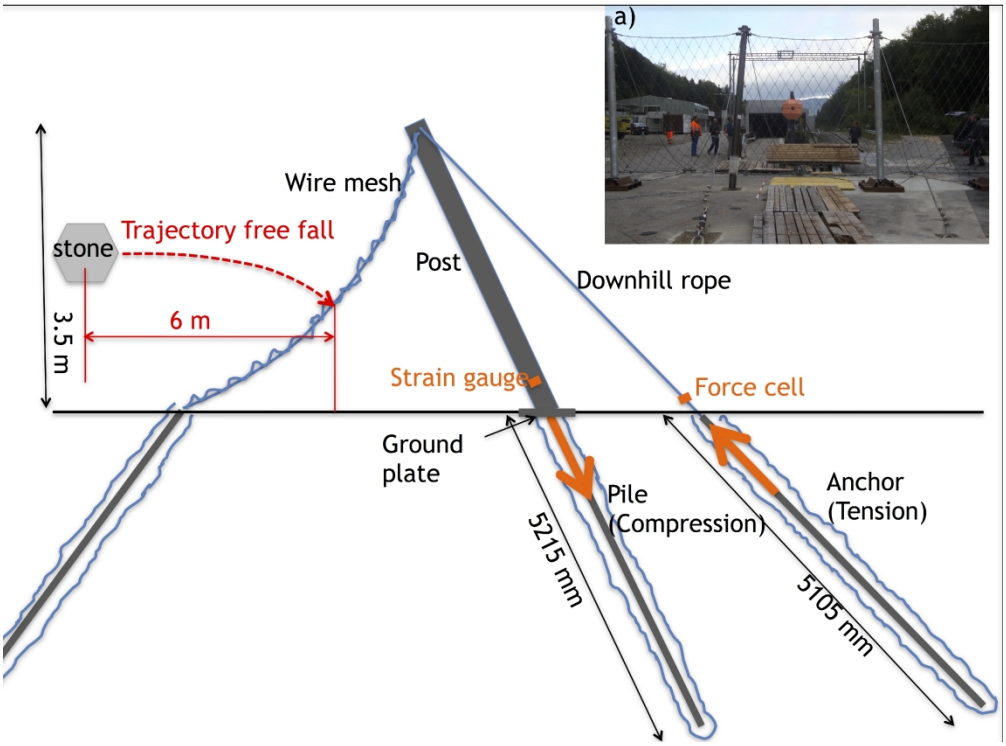

Figure 1 Schematic side view of a SPIDER Avalanche System. The arrows mark the directions of loading along the instrumented pile (compression) and anchor (tension). a) shows the front view of the experiment.

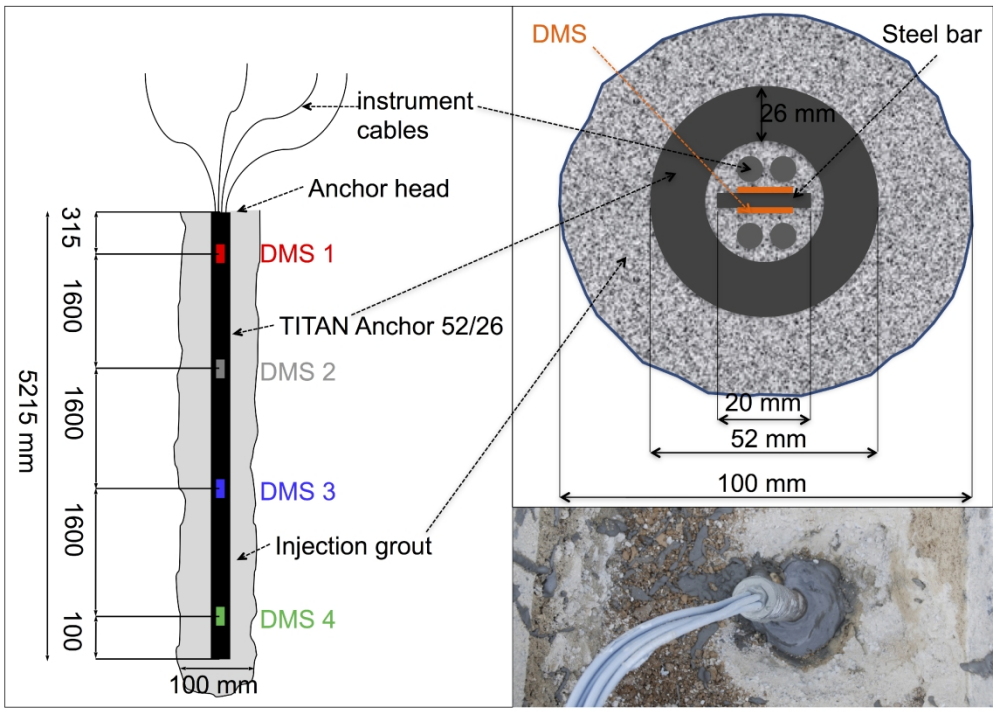

Figure 2 Left: Schematic picture of the pressure pile with specification of the positions of the strain gauges. The total length of the pile is 5215 mm. Upper Right: schematic cross-section of pressure pile and anchor. The steel rod with the strain gauges glued on it, is placed in the centre. Lower Right: Photo of grouted anchor with the measurement cables coming out at the anchor head.

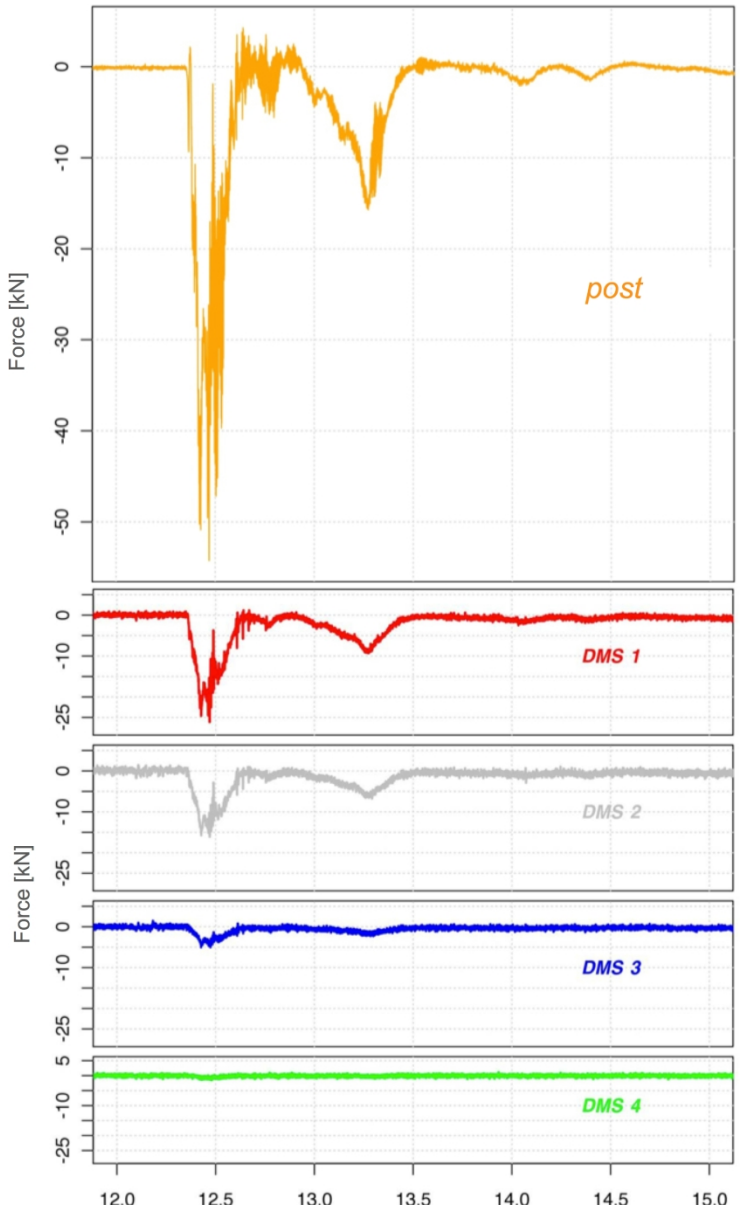

Figure 3 Time history of the measured dynamic compressive force distribution for the post and along the pile for Experiment 2 with an effective absorbed kinetic energy of 108 kJ.

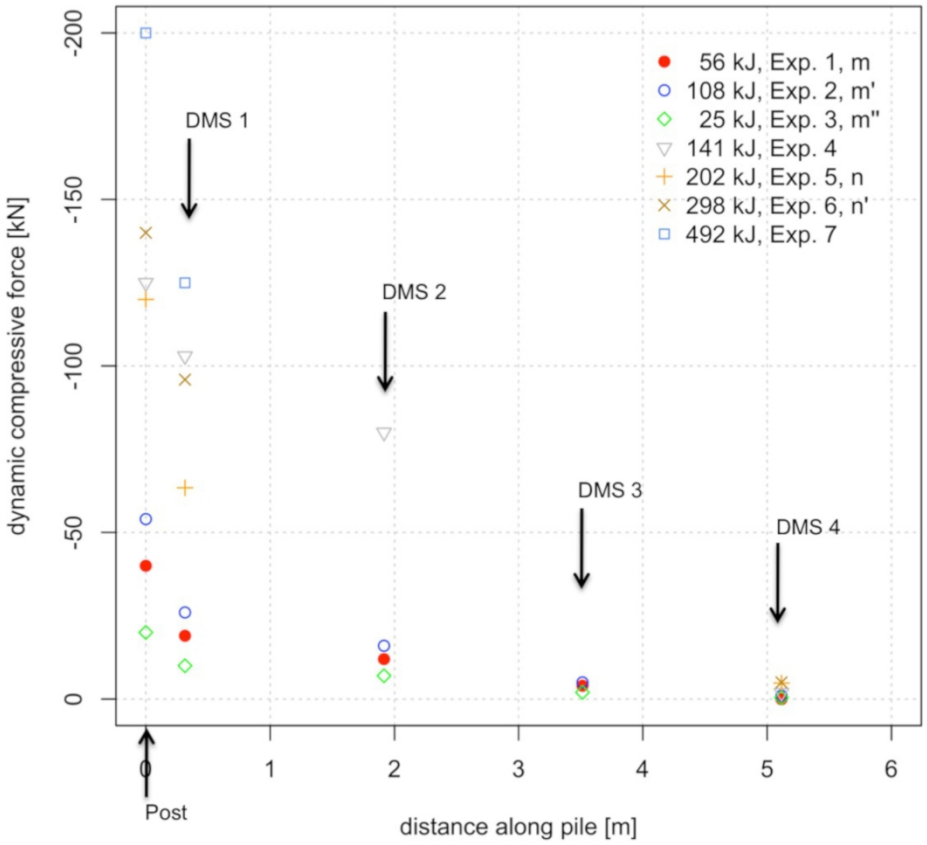

Figure 4 Measured maximum dynamic compressive forces on the foot of the post and along the pile for seven experiments with effective absorbed kinetic energies of the net. m' and m'' indicate that those experiments are multiple impacts of the setup of experiment m. n' indicates that the experiment is a multiple impact of the setup of experiment n.

182x168mm (300 x 300 DPI)

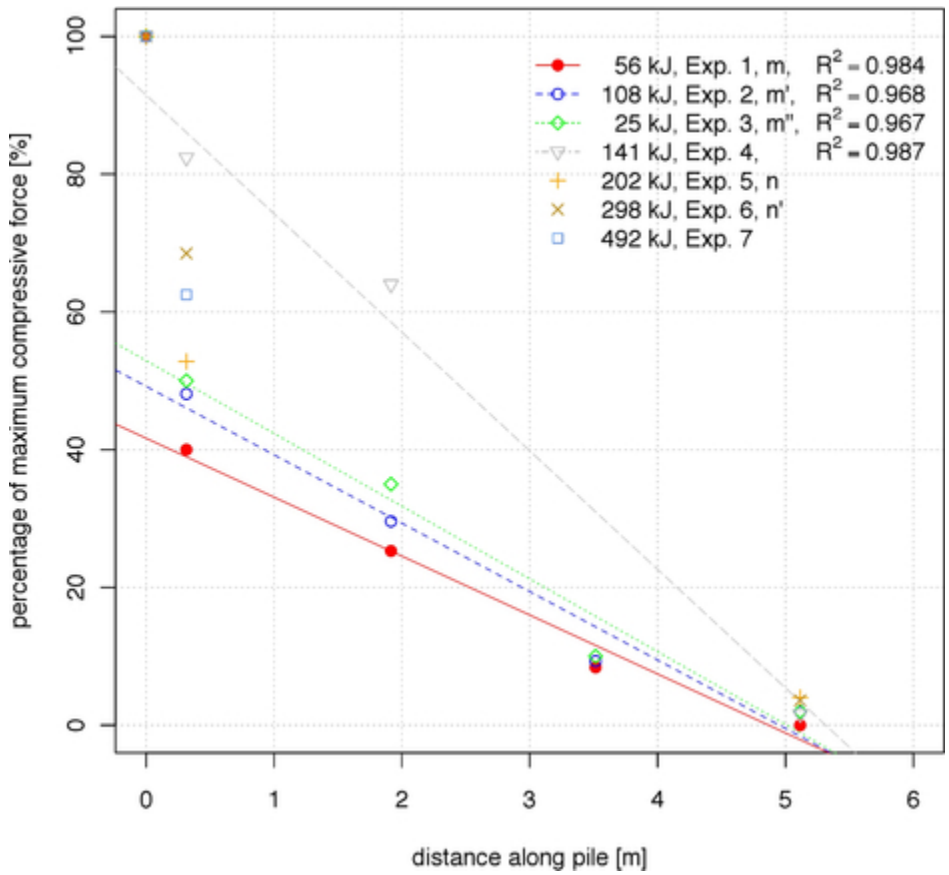

Figure 5 Percentage of the maximum compressive force along the length of the pile for effective absorbed kinetic energies of the net. The reference value, where the 100 percent are attributed to, is the force measured in the post. m' and m'' indicate that those experiments are multiple impacts of the setup of experiment m. n' indicates that the experiment is a multiple impact of the setup of experiment n. A linear regression is calculated for the measurements with minimum three points and the multiple R squared values are shown in the legend.

39x36mm (300 x 300 DPI)

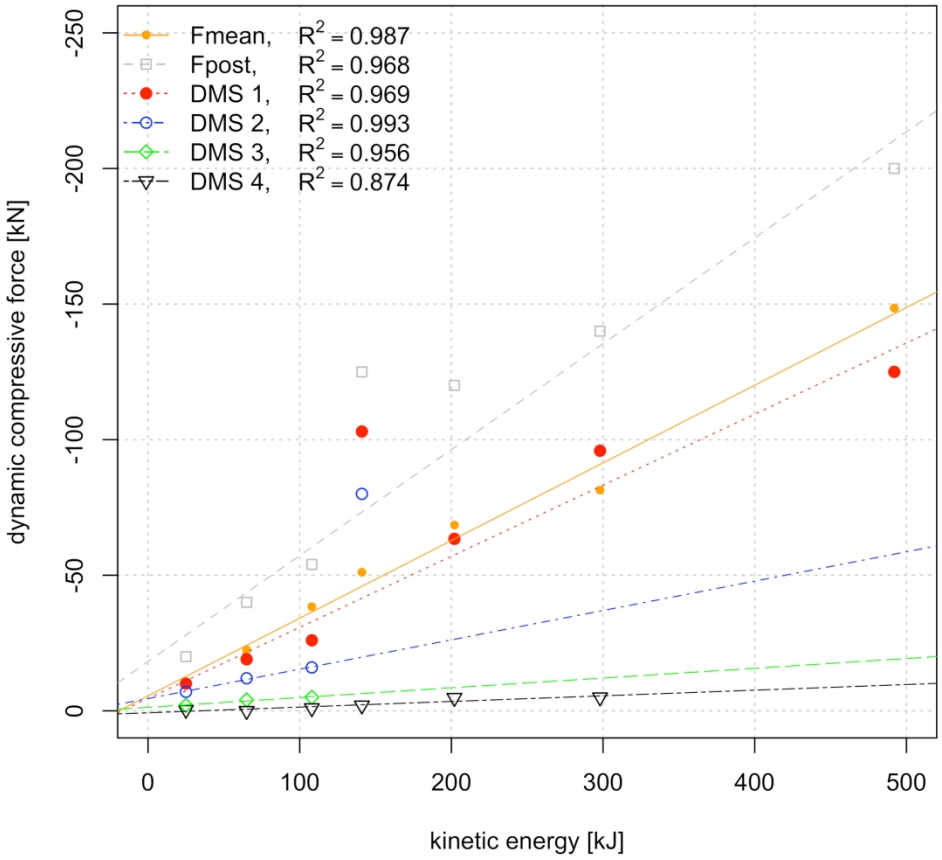

Figure 6 Maximum dynamic compressive forces of the post and the pile over the kinetic impact energy. A linear regression is calculated for the measurements with minimum three points and the multiple R squared values are shown in the legend.

182x182mm (300 x 300 DPI)

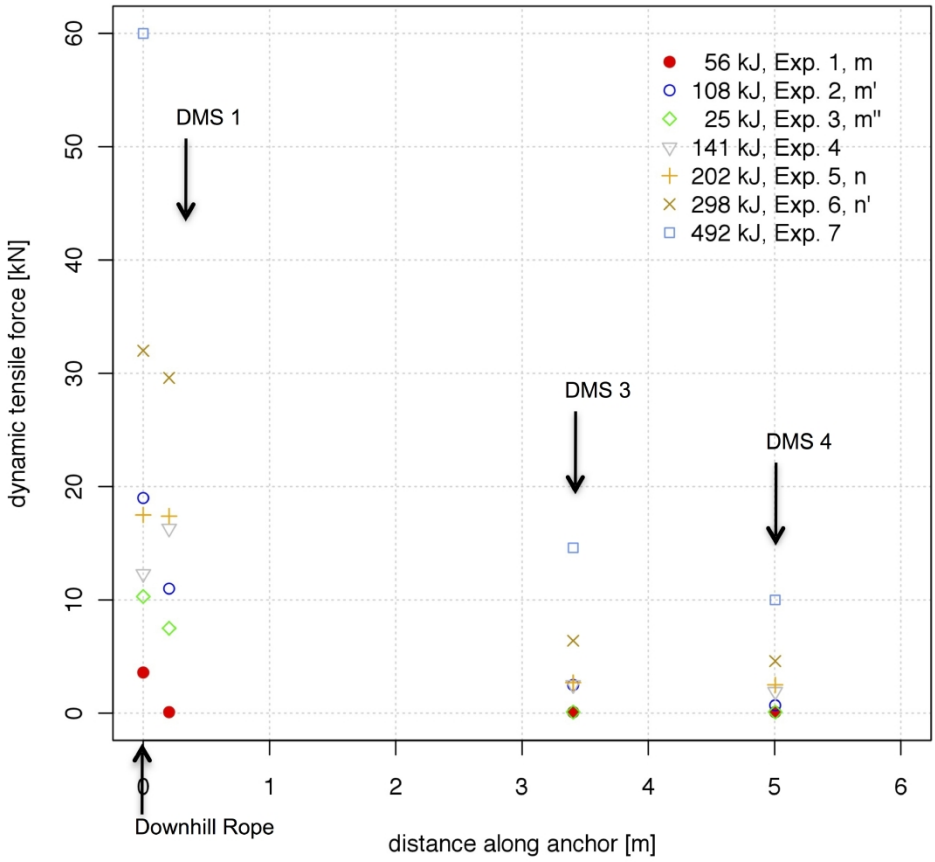

Figure 7 Measured maximum dynamic tensile forces on the rope and along the anchor for seven experiments with effective absorbed kinetic energies of the net. m' and m'' indicate that those experiments are multiple impacts of the setup of experiment m. n' indicates that the experiment is a multiple impact of the setup of experiment n.

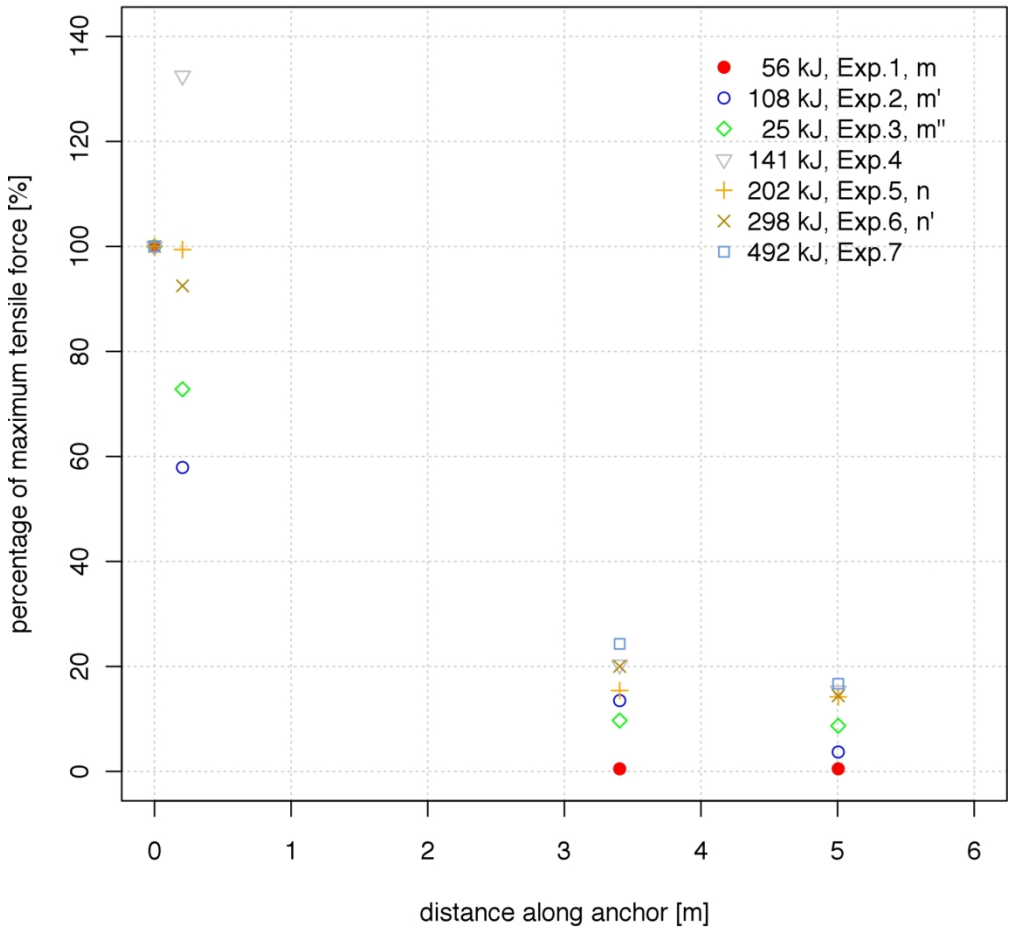

Figure 8 Percentage of the maximum tensile force along the length of the anchor for experiments with effective absorbed kinetic energies of the net. The reference value, where the 100 percent are attributed to, is the force measured in the downhill rope. m' and m'' indicate that those experiments are multiple impacts of the setup of experiment m. n' indicates that the experiment is a multiple impact of the setup of experiment n.

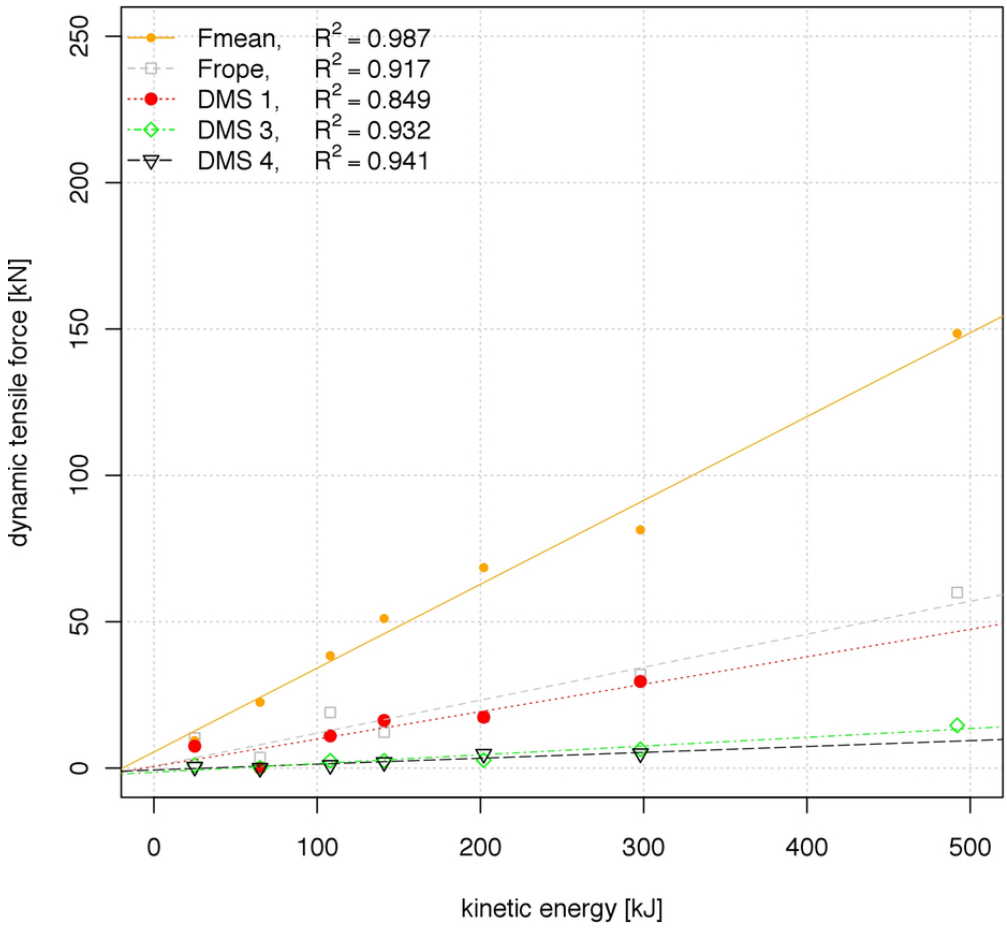

Figure 9 Maximum dynamic tensile forces in the downhill rope and the anchor over the kinetic impact energy. A linear regression is calculated for the measurements with minimum three points and the multiple R squared values are shown in the legend.

78x72mm (300 x 300 DPI)

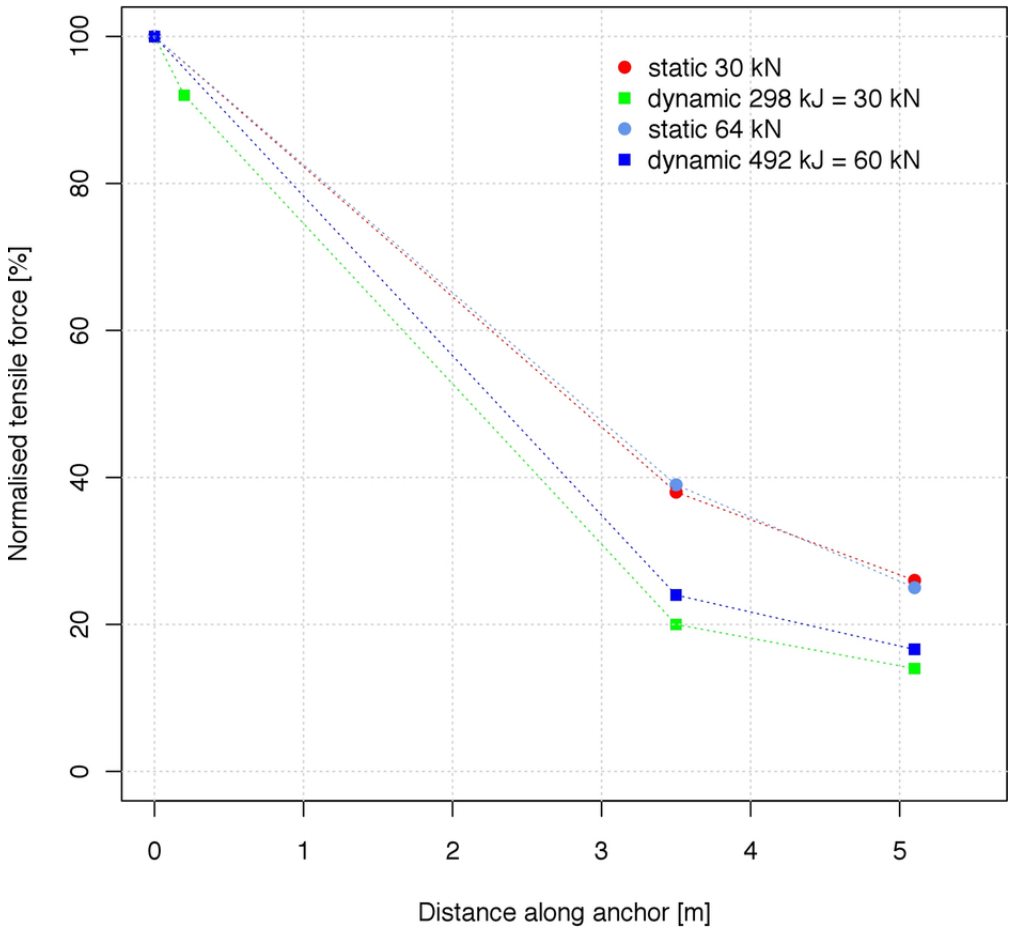

Figure 10 Comparison of the quasi-static forces from the pull loading test with the dynamic forces from experiment 6 and 7 acting along the anchor.

79x73mm (300 x 300 DPI)

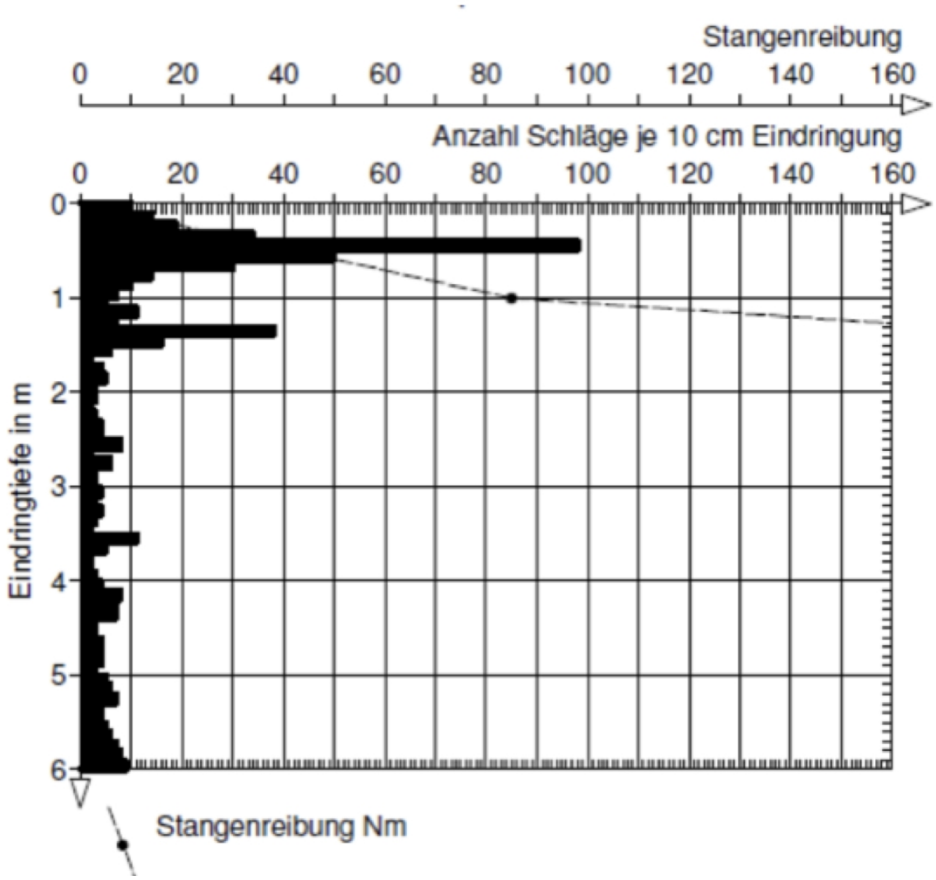

Figure A1 Data obtained from the SPT test: The amount of hits for 10 cm vertical displacement is depicted over the depth in m. The skin friction value of the tube is depicted with the dashed-dotted line.

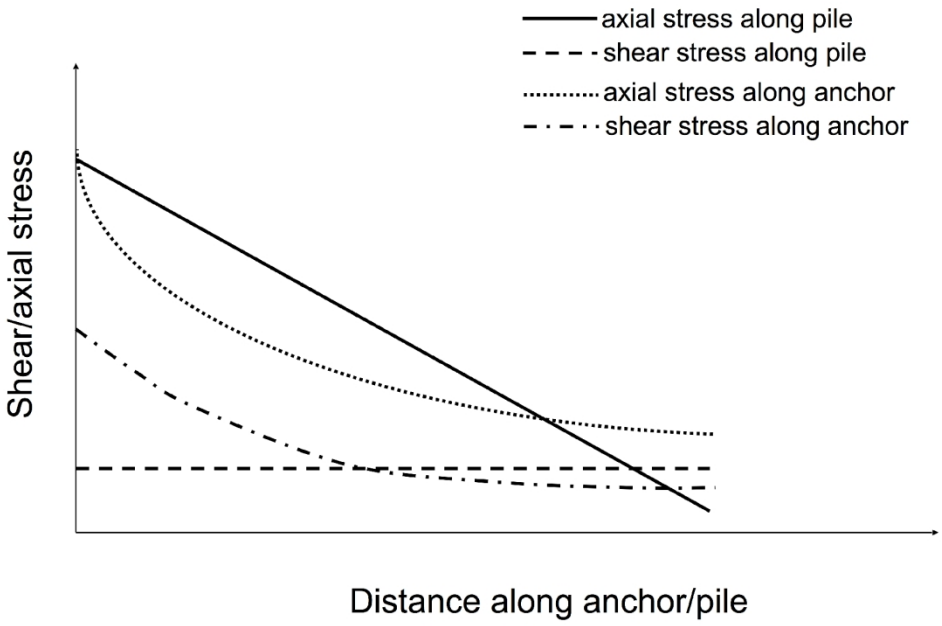

Figure A2 Schematic sketch of the stress distribution along the length of an anchor/pile during dynamic loading.

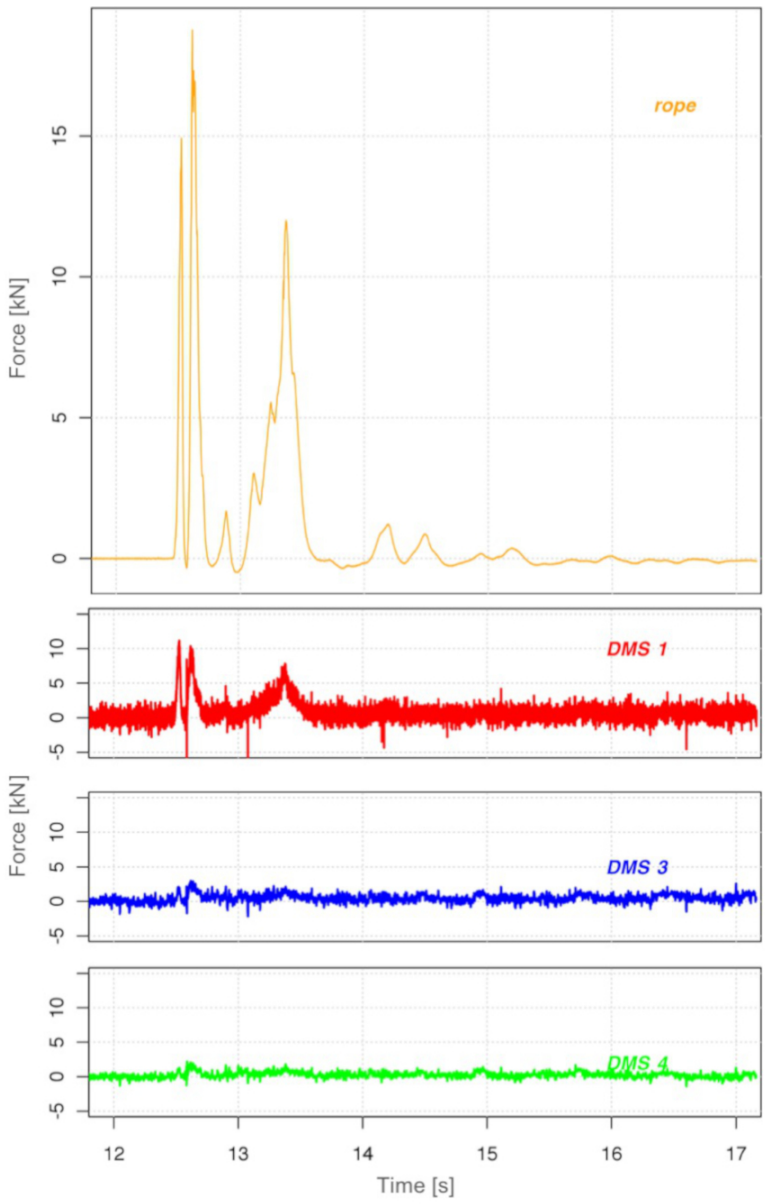

Figure A3 Time history of the measured dynamic tensile force distribution for the downhill rope and along the anchor for Experiment 2 with an effective absorbed kinetic energy of 108 kJ.

86x112mm (300 x 300 DPI)

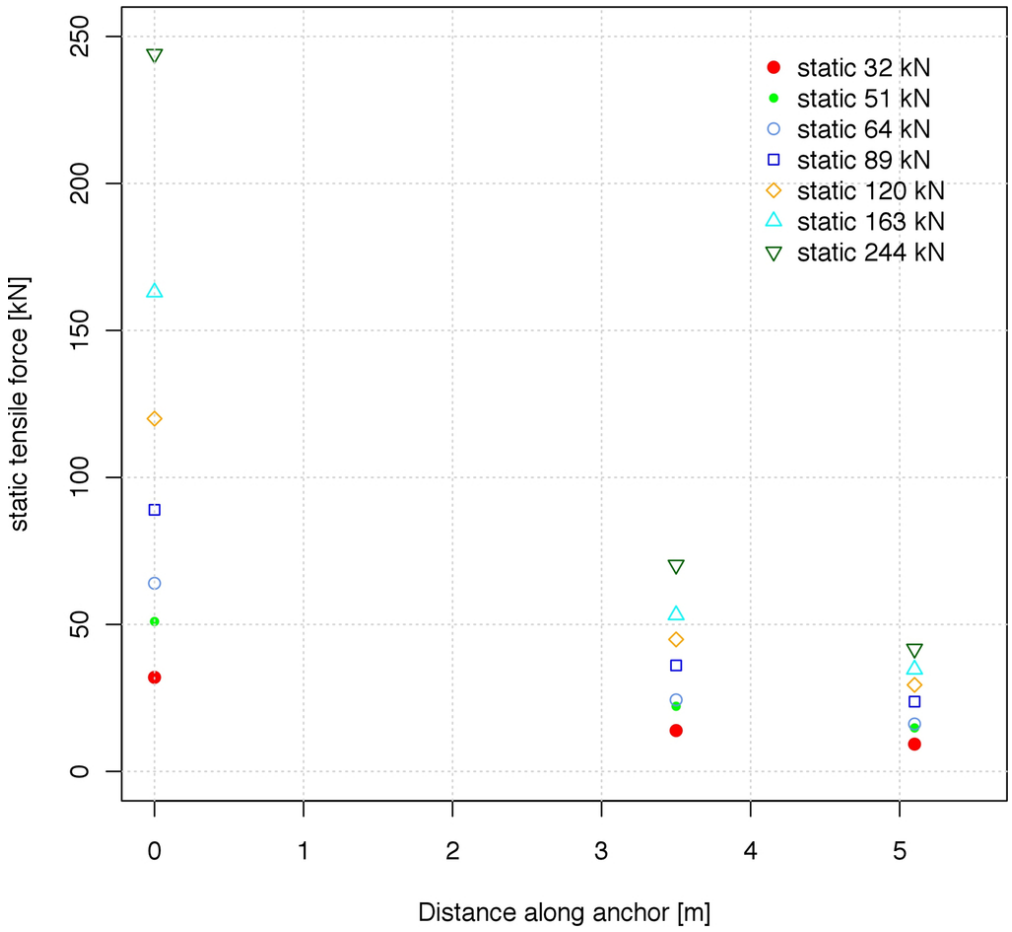

Figure A4 Measured maximum static tensile forces on the rope and along the anchor for each load step of the static pull loading test.

85x79mm (300 x 300 DPI)

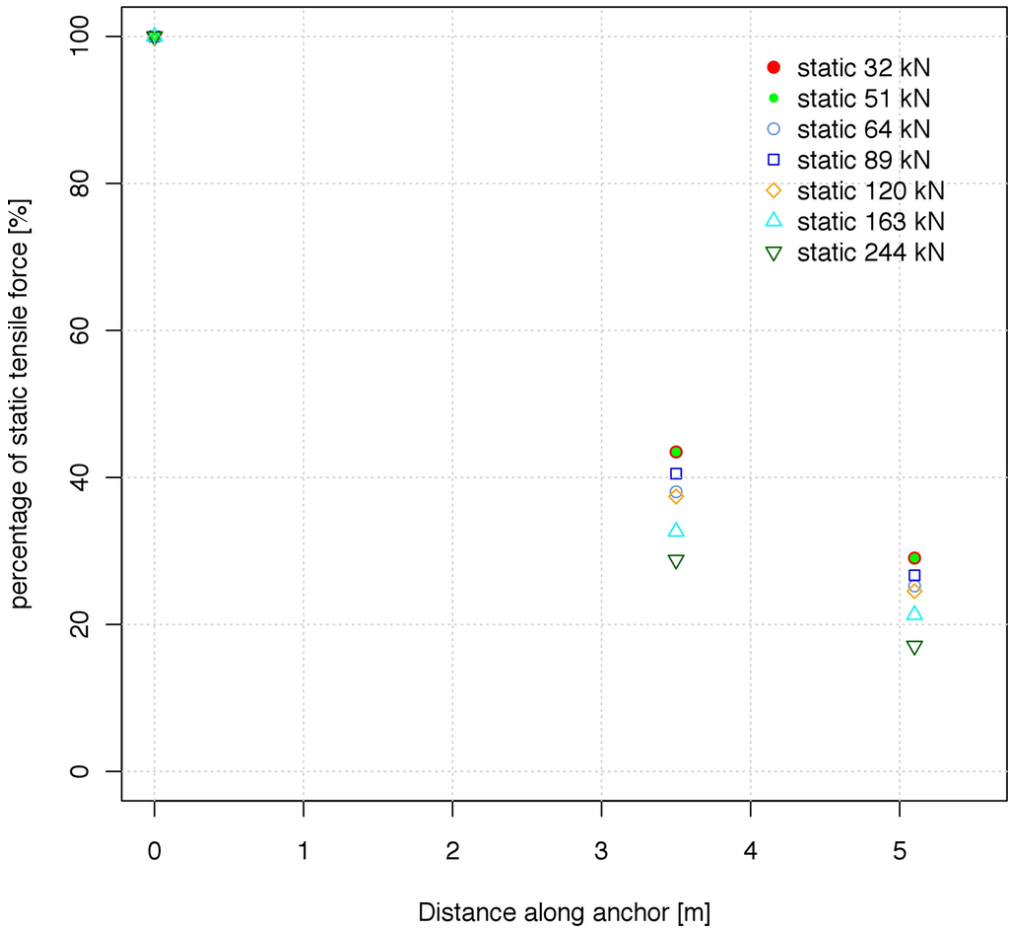

Figure A5 Percentage of the maximum static tensile forces on the rope and along the anchor for each load step of the static pull loading test.

85x79mm (300 x 300 DPI)